Interstellar catalysts and the PAH universe

Campisi, D.

CHAPTER 2

SUPERHYDROGENATION OF PENTACENE: THE REACTIVITY OF ZIGZAG-EDGES

D. Campisi, F. D. S. Simonsen, J. D. Thrower, R. Jaganathan, L. Hornekær, R. Martinazzo and A. G. G. M. Tielens, *Phys. Chem. Chem. Phys.*, **2020**, *22*, 1557-1565

Abstract. Investigating the hydrogenation of carbonaceous materials is of interest in a wide range of research areas including electronic device development, hydrogen storage, and, in particular, astrocatalytic formation of molecular hydrogen in the universe. Polycyclic Aromatic Hydrocarbons (PAHs) are ubiquitous in space, locking up close to 15% of the elementary carbon. We have used thermal desorption measurements to study the hydrogenation sequence of pentacene from adding one additional H to the fully hydrogenated pentacene species. The experiments reveal that hydrogenated species with an even number of excess H atoms are highly preferred over hydrogenated species with an odd number of H atoms. In addition, the experiments show that specific hydrogenation states of pentacene with 2, 4, 6, 10, 16 and 22 extra H atoms are preferred over other even numbers. We have investigated the structural stability and activation energy barriers for the superhydrogenation of pentacene using Density Functional Theory. The results reveal a preferential hydrogenation pattern set by the activation energy barriers of the hydrogenation steps. Based on these studies, we formulate simple concepts governing the hydrogenation that apply equally well for different PAHs.

2.1. Introduction

Polycyclic aromatic hydrocarbons (PAHs) are an important class of carbon bearing molecules which are ubiquitous in the universe and lock up close to 15% of the cosmic carbon.[105] PAHs also play an important role in the chemistry of space.[8] The role of PAHs in the formation of H_2, the most abundant molecule in the universe, in the interstellar medium (ISM) has been studied extensively.[17,41,109–112] PAHs are of general interest to the scientific community due to their pollutant and carcinogenic properties in terrestrial environments.[113] In this context, the reduction (hydrogenation) sequence that leads to the formation of aliphatic compounds[114] and the reduction of PAHs by metal free catalysts[115] have been studied, showing that the hydrogenation of these compounds leads to a less toxic mixture of saturated and unsaturated species. Owing to their photo-physical and structural properties, PAHs are also of interest for applications in hydrogen storage[116] and in optoelectronic devices.[117–120]

In this work, we focus, specifically, on one specific kind of linear catacondensed PAH, pentacene ($C_{22}H_{14}$), representative of a class called acenes. These compounds, consisting of a linear row of condensed six membered rings,[121] are characterized by zig-zag edges and they are representative of the smallest graphene nanoribbon. Zig-zag edges are a structural repetition of carbon atoms already bound to a single hydrogen atom, well known in the literature as "solo sites",[26] and bridge carbon atoms that are not bound to any hydrogen atoms. The zig-zag edges are important in astrophysics since they have strong infrared signatures that have been clearly detected in astronomical spectra.[122]

In contrast to catacondensed PAHs such as the acenes, some pericondensed PAHs (*e.g.* coronene) have no zigzag edges and their structure is characterized by duo carbons (two adjacent hydrogenated carbon sites) with strong CH modes in the 12-13 μm range.[29,123] Both catacondensed and pericondensed PAHs are susceptible to hydrogenation by hydrogen atoms under interstellar conditions, but the hydrogenation sequence differs due to their different structures.[18,40] For instance, a recent study demonstrated that the hydrogenation sequence of coronene, a pericondensed PAH, starts from the duo carbons[40] with delayed hydrogenation of the other carbon sites. For catacondensed species, the hydrogenation sequence begins from the central aromatic ring, saturating both inner and edge carbons.[18,124]

Superhydrogenated PAHs are important since they might be responsible for the formation of molecular hydrogen in Photodissociation Regions (PDRs).[125] PDRs are regions where the ultraviolet radiation from nearby bright stars influences the chemical and physical properties of the present molecular structures.[34] It is well appreciated that, because of the high UV flux, molecular hydrogen has to be rapidly reformed and that the normal routes considered for H_2 formation in the ISM do not suffice to account for its observed abundance.[33,126] As astronomical observations have revealed a spatial correlation between the H_2 formation rate and interstellar PAHs emission in these regions, PAHs have been suggested as possible catalysts for H_2 formation.[126,127] Different mechanisms have been studied in order to understand the formation of molecular hydrogen on PAHs, including reactions between two chemisorbed atomic hydrogen atoms through Langmuir-Hinshelwood (LH) and Eley-Rideal (ER) mechanisms. These mechanisms have been studied for pyrene[128] and for coronene,[17,110] demonstrating that Eley-Rideal abstraction is a viable pathway for PAH catalyzed molecular hydrogen formation. Moreover, Rasmussen[124] studied the correlation of the increase in hydrogen binding energy with increasing zigzag edge length, using several acenes with different length as models. Therefore, it is crucial to study the aromatic–aliphatic character of PAHs when they are in a hydrogen rich environment in order to shed light on the sequence that leads to the so called “Magic Numbers” in the hydrogenation sequence of these species.[129]

This study aims to determine and understand the hydrogenation sequence of pentacene that leads to complete superhydrogenation of the molecule, using a combination of experimental and theoretical techniques. Specifically, temperature programmed desorption (TPD) is employed to directly determine the sequence of products of hydrogen addition to pentacene while density functional theory (DFT) calculations are used to investigate the hydrogenation sequence. This also serves as a test of simple concepts that may be applicable to other aromatic species featuring a bipartite lattice (*e.g.* carbon sp^2 structured as a graphene lattice).

2.2. Experimental and Theoretical Methods

2.2.1. Thermal Desorption Measurements

Experimental investigations of superhydrogenation of pentacene were conducted using temperature programmed desorption (TPD) measurements under ultra high vacuum (UHV) conditions; $p < 10^{-9}$ mbar. A few multilayers of commercially available pentacene ($C_{22}H_{14}$; Sigma-Aldrich; triple-sublimed grade, ≥99.995%) were deposited onto highly oriented pyrolytic graphite (HOPG), held at 290 K, using a home-built Knudsen-type effusion cell. The HOPG substrate was cleaved in air prior to mounting and then annealed in UHV to 1100 K before each measurement. Typically 2-3 pentacene multilayers were obtained after 2 minutes deposition with the molecular doser at 135 °C (408 K). A monolayer could then be consistently produced by annealing the sample to 330 K for 5 minutes, removing the multilayers.

The monolayer of pentacene on HOPG was then exposed to a beam of atomic hydrogen (H) using a hydrogen atom beam source (HABS).[130] The HABS was operated at ≈ 2200 K, producing a hot atomic H beam which was subsequently cooled collisionally, through a quartz nozzle, to an estimated temperature of ≈ 1400 K.

TPD measurements were performed with a linear ramp of β =1 K s^{-1} until reaching 1100 K. To mass-selectively detect the species that leave the surface a quadrupole mass spectrometer (QMS) (Extrel CMS LLC) was used, scanning the range 258-340 atomic mass units (amu)/charge. The

TPD spectra within the given mass range are integrated and averaged over the relevant desorption temperature range to give the presented mass spectra.

2.2.2. Density Functional Theory Calculations

Theoretical investigations were conducted using density functional theory (DFT) as implemented in the Gaussian 16 software suite.[131] In order for our calculations to have sufficiently high accuracy, we used the exchange correlation functional M06-2X.[77] This functional has been proven to provide an accurate description of PAHs hydrogenation since it has been found to be in close agreement with coupled-cluster calculations.[40] All calculations were carried out using the unrestricted (UHF) formalism. We employed the new pcseg-1[132] basis set, a segmented polarization consistent double zeta basis set optimized for DFT. All geometries were optimized using the Berny algorithm[133] and, in order to characterize the minima and saddle points, normal modes were analyzed within the harmonic approximation. All energies were corrected in order to reduce the basis set superposition error (BSSE) using the counterpoise scheme[100,134] implemented in Gaussian 16. We employed the molden[135,136] software package to visualize molecular structures and normal modes.

The theoretical part of this work is divided into two sections: the first describes the sequence of H addition that leads to fully hydrogenated pentacene while the second describes the hydrogenation sequence of superhydrogenated species based on a binding energy and energy barrier analysis.

The binding energies are defined as:

$$E_{bind} = [(E_{\mathrm{H}} + E_{\mathrm{reagent}}) - E_{n\mathrm{H-pentacene}}] \tag{2.1}$$

E_{bind} is the binding energy, E_{H} is the energy of atomic hydrogen in gas phase, E_{reagent} is the energy of the reactant that is interacting with the atomic hydrogen. Positive values of binding energies indicate exoergic processes, while negative values indicate endoergic ones.

The energy barriers are defined as:

$$E_{bar} = [E_{\mathrm{TS}} - (E_{\mathrm{H}} + E_{\mathrm{reagent}})] \tag{2.2}$$

E_{bar} is the energy barrier, E_{TS} is the energy of the transition state structure calculated as a first order saddle point, while E_{H} and E_{reagent} are the energy of the minima for the hydrogen atom and reactant, respectively. For the definition of transition state, the energy barrier is always positive.

Finally, the formation energy is defined as:

$$E_f = [E_{\mathrm{product}} - (E_H + E_{reagent})] \tag{2.3}$$

E_{f} is the formation energy, E_{product} is the energy of the product, while E_{H} and E_{reagent} are the energies of the hydrogen atom and reactant, respectively. In the case of the formation energy, negative values indicate exoergic processes, whereas positive values indicate endoergic ones. For simplicity, we label the hydrogenated species of pentacene as nH-pentacene where n is a whole number (*e.g.* 3H-pentacene, is pentacene with 3 extra hydrogen atoms attached, namely $C_{22}H_{17}$). We use the term *syn* (*cis* position) when the extra hydrogen are chemisorbed on the same side of the molecule, while, we use the term *anti* for the hydrogens chemisorbed on opposite sides (*trans* position).

In order to gain broader insights into the hydrogenation process, the sequence of hydrogenation was rationalized with simple concepts derived from a tight-binding model where the most reactive site is related to the smallest π-coordination number (number of carbon atoms connected to a carbon center) and the highest hypercoordination number (number of second carbon atom neighbours that have the same coordination number) for closed-shell systems.[137] Attaching a hydrogen on a closed-shell system (*i.e.* all odd extra hydrogens chemisorbed) generates an unpaired electron (mid-gap state) that localizes preferentially in the *ortho-* or *para*-positions respect to the already extra hydrogen attached. Therefore, the odd hydrogenations were predicted using the coordination and hyper-coordination rule, whereas the even hydrogenations were predicted using the *ortho–para* localization. Finally, these simple rules were confirmed through the binding energy and energy barrier analysis. The latter are correlated by the Bell–Evans–Polanyi principle according to which larger energy barriers are associated with lower binding energies.[138,139]

2.3. Experimental Results

In Fig. 2.1, mass spectra for pentacene monolayers exposed to increasing H atom fluences are displayed. The initial mass spectrum before hydrogenation can be seen in Fig. 2.1(a). In the mass spectrum prominent peaks are seen at masses: 278 amu (the pentacene molecule, $C_{22}H_{14}$), 280 amu (6,13-dihydropentacene (DHP), $C_{22}H_{16}$), 294 amu (6-hydroxypentacene $C_{22}H_{14}O$), and 308 amu (pentacenequinone (PQ), $C_{22}H_{12}O_2$). Mass 279 contains contributions from both the fragmentation of DHP during the ionization step in the QMS and from pentacene with the naturally occurring isotope ^{13}C (^{13}C is also seen in DHP as mass 281 in Fig. 2.1(a)). All masses detected below 278 amu, *e.g.* 276 amu, are ascribed to fragmentation in the QMS. The commercially available pentacene batches are known to have the oxidized species PQ as a main contaminant,[140] and more oxidised and/or superhydrogenated species are known to form when pentacene is exposed to air and light.[141] DHP is also present in commercially available pentacene and is known to be a byproduct of sublimation.[142]

Fig. 2.1(b)-(e) show the mass distribution of superhydrogenated pentacene after hydrogenation times of b) 180 s, c) 900 s, d) 1800 s and e) 54000 s (17 hours). Fig. 2.1(b) shows a small degree of hydrogenation

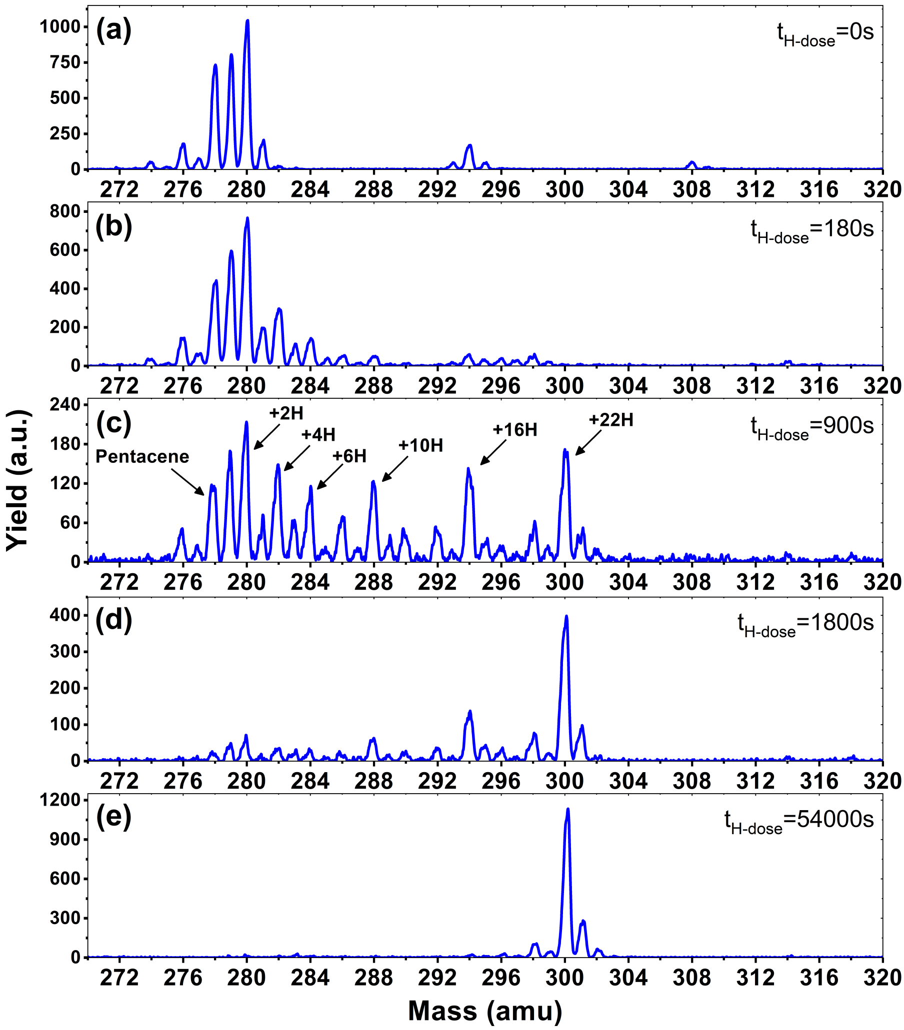

Figure 2.1: Mass spectra showing the mass distribution of a pentacene monolayer after different H-atom exposure times presented in the figure. (a) Mass distribution of a monolayer of pentacene (mass 278) with the prominent contaminants dihydropentacene (mass 280) and 6-hydroxypentacene (mass 294). (b)-(e) Mass distributions shifting towards higher masses with increasing H atom fluences, eventually reaching mass 300 corresponding to fully superhydrogenated pentacene.

for both the pentacene and the oxidized species. The species with even masses such as 280, 282 and 284 are seen to be more prominent than the odd. This is consistent with the fact that superhydrogenated pentacene molecules with an odd mass will be open-shell, and hence exhibit a radical behaviour and therefore be more reactive towards the addition of a subsequent H atom. By contrast, the even mass species are less prone to further hydrogenation. The odd-even oscillation is clearly visible in Fig. 2.1(c) where the mass distribution covers the entire range from pristine pentacene, mass 278, to fully superhydrogenated pentacene, $C_{22}H_{36}$, with mass 300. While the odd-even oscillation is clearly visible, it is also evident that some specific species (with specific superhydrogenation degrees) appear more prominently than others. The most prominent species are: 280 (+2H), 282 (+4H), 284 (+6H), 288 (+10H), 294 (+16H) and 300 (+22H), also indicated in Fig. 2.1(c).

After extended H atom exposure, see Fig. 2.1(d)-(e), the mass distribution is pushed towards mass 300, corresponding to fully superhydrogenated pentacene $C_{22}H_{36}$. In Fig. 2.1(e) the peak at mass 300 completely dominates the spectrum. The smaller peaks seen at masses 301-302 and 298-299 are ascribed to the ^{13}C isotope and fragmentation in the QMS, respectively. Hence, the fact that it is possible to drive the entire mass distribution to fully superhydrogenated pentacene for long H deposition times (see Fig. 2.1(e)) reveals that H atom addition reactions dominate over H atom abstraction for superhydrogenated pentacene.

2.4. Theoretical Results

2.4.1. Hydrogenation Sequence

The hydrogenation sequence found for pentacene is schematically shown in Fig. 2.2. At the first hydrogenation, the carbon sites more inclined to be hydrogenated are C1 and C6 (Fig. 2.3(a)) with the highest hyper-coordination. The least inclined carbon atoms to be hydrogenated are the inner carbons C5 and C14 (Fig. 2.3(a)) since they have the highest coordination numbers. The carbon atoms C13 and C12, have intermediate propensity to be hydrogenated (a detailed description of the sequence is reported in the Appendix). The first hydrogenation and all odd hydrogenation steps are the single addition of a hydrogen atom to a closed-shell species and are, therefore, associated with the formation of a mid-gap state (singly occupied molecular orbital) which is represented schematically in Fig. 2.3(b). The mid-gap state generated is in a radical open-shell system and will react readily with a radical species such as a further hydrogen atom. The mid-gap state formation increases the electron affinity of the carbon sites where an unpaired electron is localized, but this affinity decreases as the distance from the hydrogenated carbon sites increases.[137] For instance, the highest probability that an atomic hydrogen will be chemisorbed are those carbon sites nearby the already extra hydrogen chemisorbed. This tendency is illustrated in Fig. 2.3(b). Hence,

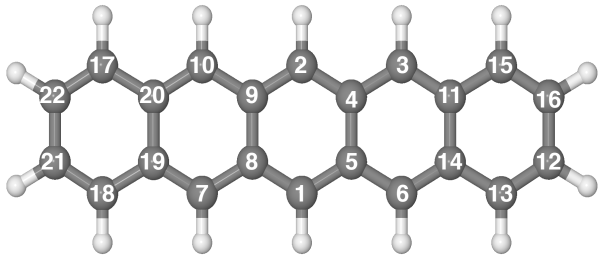

Figure 2.2: Optimized molecular structure of pentacene in balls and sticks. The numerical labels reported indicate the full hydrogenation sequence of pentacene.

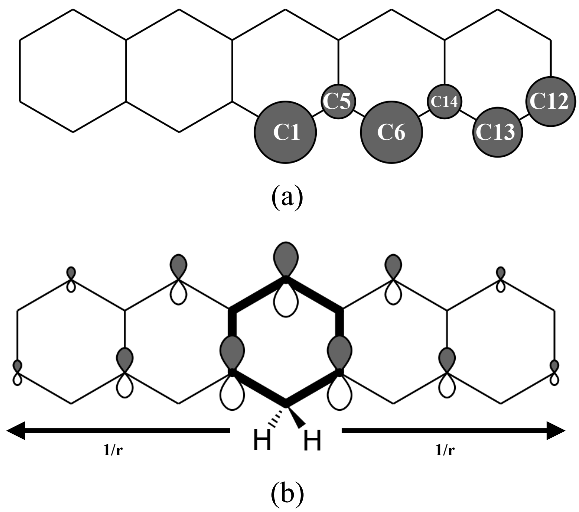

Figure 2.3: (a) Schematical representation of the affinity of the carbon atoms to be chemisorbed by the first hydrogen atom. Larger balls indicates higher hydrogenation affinity. (b) Graphical representation of localized mid-gap states for the second hydrogenation. The arrows show decreasing effect of mid-gap state with increasing distance from the first hydrogenated carbon site.

for even hydrogenation reactions, the sequence is led by *ortho-para* localization of the unpaired electron by the mesomeric effect with respect to the already chemisorbed extra hydrogen. Therefore, the mid-gap state drives the reactivity to specific carbon sites in the molecule. The second atomic hydrogen might chemisorb in *ortho* or in *para* with respect to the already chemisorbed extra hydrogen (Fig. 2.3(b)).

The hydrogenation sequence follows a simple rule: first hydrogenation of the carbon in the solo position (CH bonded H where adjacent C atoms do not have a H), followed by hydrogenation of the neighboring inner carbons (bridge carbons). The latter step reflects that an inner carbon is under-coordinated upon hydrogenation of a neighbour carbon site. This is in line with the study carried out by Klærke *et al.*[143] and Bonfanti *et al.*[137] confirming that it is easier to hydrogenate edge carbons than bridge ones.

The highest binding energy found is associated with the chemisorption of the extra hydrogen in position 2 (Fig. 2.2), which is *para* with respect to carbon 1. Once carbons 1 and 2 are hydrogenated, two topologically disconnected systems are generated. The molecule now consists of two naphthalene units, bound to the hydrogenated non-aromatic ring, outlined in bold in Fig. 2.4(a). These two naphthalene units are equivalent

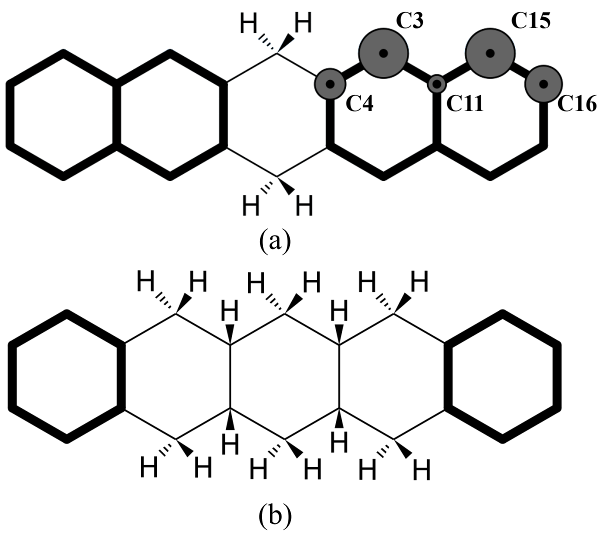

Figure 2.4: (a) Graphical representation of disconnected naphthalene units and their propensity to be hydrogenated. (b) Graphical representation of disconnected benzene units.

and therefore, we considered the chemisorption of the third hydrogen atom on C3 (Fig. 2.4(a)) which has the highest hyper-coordination. Fig. 2.4(a) also reports graphically the propensity of the carbon atoms to be hydrogenated (details reported in the Appendix) where it is clearly shown that

C3 and C15 have higher affinity (high hyper-coordination) compered to the inner carbon site C11 as the latter has the highest coordination number, while, C16 and C4 have lower propensity to be hydrogenated since these carbon sites have lower hyper-coordination. The fourth hydrogen atom, then, chemisorbs on the least coordinated carbon site (labeled C4 in Fig. 2.4(a)) that is a bridge carbon one. The sequence, schematically shown in Fig. 2.2, continues with the system tending to preserve the aromaticity of individual rings as long as possible. Moreover, during the hydrogenation, disconnected systems are created, as naphthalene and benzene rings (shown in bold in Fig. 2.4(b)), and the hydrogenation sequence might change accordingly. A complete overview of the sequence is reported in the Appendix.

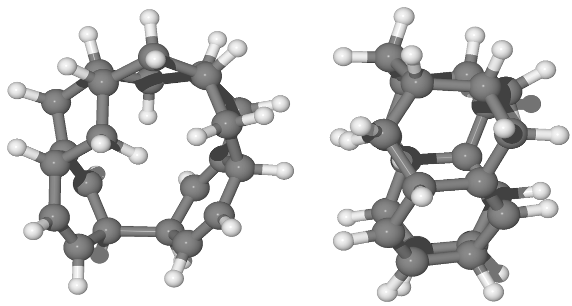

Figure 2.5: Front view and side view, respectively, of the optimized molecular structure in balls and sticks of quasi-nanotube formed by the chemisorption of 12th hydrogen on a less reactive carbon site of *syn*-11H-pentacene (see section 12th Hydrogenation in the Appendix).

2.4.2. *Syn* and *Anti* Conformation

In our experiments, a pentacene molecule is exposed to a flux of hydrogen atoms on only one side as the monolayer is deposited on a graphite surface. Therefore, one could argue, from a geometric perspective, that superhydrogenation only occurs on one side. Initially, we studied the reaction sequence by chemisorbing hydrogen atoms on single side of the molecule (*syn* path). The complete hydrogenation of pentacene leads to the formation of a bent structure as reported in Fig. 2.7. As it may be relevant for the hydrogenation of gaseous pentacene, we also considered binding the hydrogen atoms to the bridging carbon atoms of the molecule on alternat-

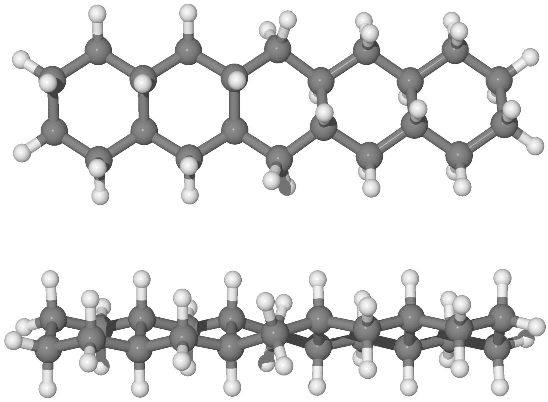

Figure 2.6: Side view and top view of optimized molecular structure of *anti*-22H-pentacene in balls and sticks.

ing sides of the molecular plane (*trans*-hydrogenation), referred to here as "*anti* position", and shown in Fig. 2.6. The *anti* conformation in the case of pentacene is relevant only in carbon sites where no hydrogen atoms are already bound. In fact, in the case of edge carbons where two hydrogen atoms are attached, the hydrogen atoms are topologically equivalent.

The hydrogenation sequence for the *anti* path begins with the 4th hydrogenation since the hydrogen atoms already chemisorbed are topologically equivalent. Specifically, the hydrogen atom may chemisorb on carbon 4 (Fig. 2.2) from the bottom side with respect to the plane of the molecule. The addition of the next hydrogen atom to carbon 5, proceeds from the top of the molecule with respect to the molecular plane. Hence, if the hydrogen atom chemisorbs on the bottom side of the molecule, specifically on carbon atoms 4, 8, 11 and 20, we can observe a more linear structure with all rings in arm-chair conformation. A complete description of why those hydrogenated species are formed, based on the analysis of binding energies and energy barriers, is reported in the next section and a more complete description of the sequence is reported in the Appendix.

2.4.3. Quasi-Nanotubular Formation

Furthermore, the formation of these topologically disconnected systems may cause an intramolecular homo-coupling (*i.e.* formation of C-C bond inside the same molecule). Specifically, we found that for radical species, *syn*-9H-pentacene, *syn*-11H-pentacene, *syn*-13H-pentacene and *syn*-15H-pentacene (see Appendix), further hydrogenation takes place in the ring disconnected from the already present unpaired electron and an intramolecular radical-radical reaction will occur leading to the formation of a nanotubular structure during the chemisorption of the 12th hydrogen radical (*e.g.* that shown in Fig. 2.5). The disconnected systems do not allow the localization of the unpaired electron within the same molecule and thus results in the formation of such a nanotubular structure. As discussed in the Appendix, several nanotubular structures could be formed during the hydrogenation process.

Table 2.1: Formation energy (ΔE_f) of quasi-nanotubes from pentacene with n numbers of extra H atoms chemisorbed on the same side.

Hn	ΔE_f (eV)
10	-2.39
12	-1.20
14	-2.50
16	-2.70

Table 2.1 provides the exoergic formation energies, indicating that the formation of quasi-nanotubular structures is thermodynamically favourable, especially during the addition of the 16th hydrogen atom in a less reactive carbon site (more details are reported in the Appendix). Moreover, the formation of these nanotubular structures occurs only in the gas-phase and involves an intramolecular homo-coupling (formation of a carbon bond within a molecule). In a similar study, the formation of intermolecular homo-coupling (formation of a carbon bond between two molecules) between two pentacene molecules on Au(111), resulting from superhydrogenation, has been investigated.[144] In this case, intermolecular homo-coupling dominates on a surface. This process is not important in the gas phase as collisions are rare. Instead, in the gas phase, intramolecular nanotubular formation dominates.

2.4.4. Analysis of Superhydrogenated Species

Fig. 2.8 shows the trend of energy barrier for the *syn* and *anti* path. We do not expect energy barriers of activation for odd to even hydrogenation since 1H-pentacene is an open-shell radical ready to react through a barrier-less reaction with another radical (atomic hydrogen), which is in line with the studies conducted on coronene and pyrene.[17,40,128] From chemical principles, we expect that this is a general rule and we have focused our calculations on determining energy barriers involved in the formation of odd hydrogenated species.

***Syn* Path.** Pentacene is particularly reactive for the first two hydrogenation reactions, as indicated by the presence of 6,13-dihydropentacene (*syn*-2H-pentacene) as a contaminant in the experiments. Once *syn*-2H-pentacene is formed, hydrogenation proceeds until larger energy barriers

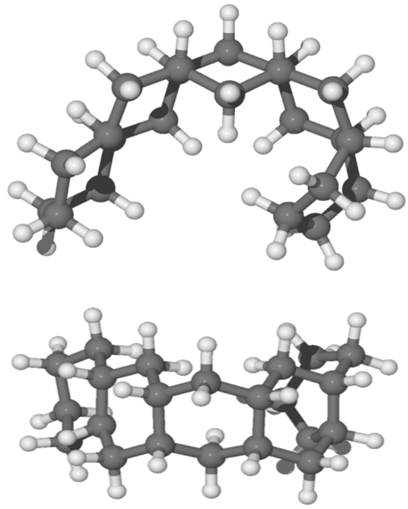

Figure 2.7: Side view and top view of the optimized molecular structure of *syn*-22H-pentacene in balls and sticks.

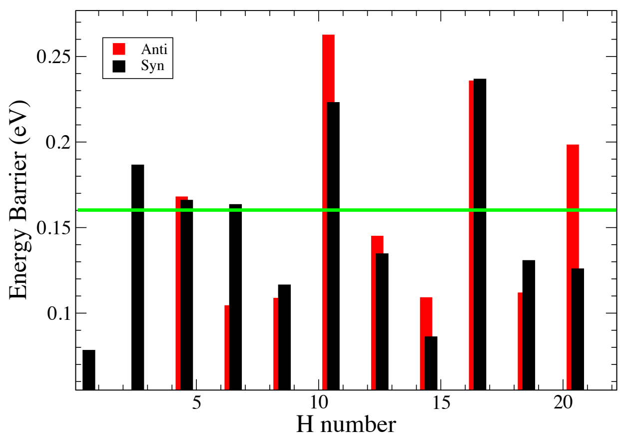

Figure 2.8: Calculated energy barriers in the hydrogenation from an even to an odd number of H's on pentacene. H number indicates the number of extra hydrogens chemisorbed on pentacene. The green line represents energy barrier relevant under our experimental conditions. Note that there is no energy barrier for the hydrogenation from an odd to an even number of H atoms.

are difficult to overcome at the experimental conditions. Specifically, energy barriers higher than 0.16 eV (green line in Fig. 2.8) are less accessible in our experiment with a 1400 K atomic hydrogen beam. In fact, the peaks related to +2H, +4H, +6H, +10H, +16H are observed in the mass spectra reflect the difficulty to overcome barrier heights for further hydrogenation processes.

Syn-21H-pentacene can react through a barrierless reaction with another radical to produce the fully hydrogenated pentacene with a mass of 300 amu. The peak corresponding to mass 300 amu becomes prominent as exposure times to atomic hydrogen increases. The presence of magic numbers in the hydrogenation of pentacene reflects that the energy barriers are particularly high whenever a new aromatic ring has to be attacked.

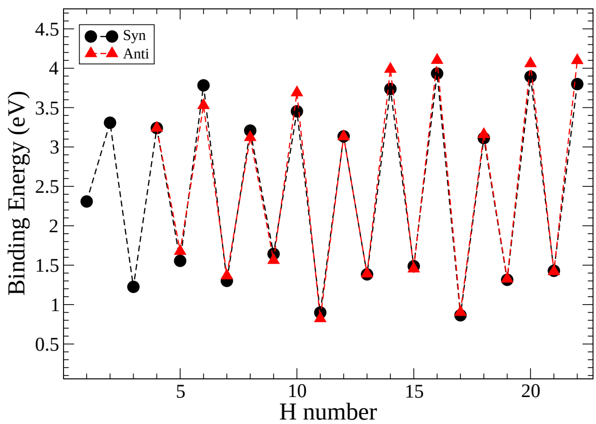

Figure 2.9: Trend of binding energies for the hydrogenation of pentacene for two different paths: *syn* and *anti*. H number indicates the number of extra hydrogens chemisorbed on pentacene.

The values of binding energies reported in Fig. 2.9 suggest that all even hydrogenated species are more favourable than the odd hydrogenated species and have binding energies between 3 and 4.5 eV. The species with an odd number of extra hydrogen atoms attached display smaller binding energies between 2.5 eV and 1 eV. This trend was studied and confirmed on several neutral PAHs,[17,124,128] while for the cation the opposite is found as expected for an open shell species.[129,145] Within the odd and even sequences there are small variations in binding energy which are due to high electron affinity of these carbon sites toward the hydrogenation. However, these differences are small and, at the temperature of the experiment, these are unlikely to be relevant for the discussion of the magic numbers.

Our study of the binding energies reveals that superhydrogenation is energetically favorable for all species. The odd-even pattern and the presence of magic numbers in the even sequence reflects the pattern of activation barriers in the production of odd species from even ones. The lowest energy barriers found in this work are related to the chemisorption of the hydrogen on aliphatic carbon and, in particular, for the case of the formation of *syn*-9H, *syn*-13H, *syn*-15H and *syn*-19H-pentacene.

***Anti* Path.** The hydrogenation sequence in gas phase space environments may reflect the fact that both sides of the pentacene molecule can be attacked by radical hydrogen atoms. Therefore, we investigated an alternative path where the hydrogen atoms chemisorbed on the bridge carbons are in *anti* conformation respect to the plane of the molecule, as shown in Fig. 2.6. The energy barriers for the addition of hydrogen atoms to the *anti* hydrogenated pentacene follow the same trend as that of the *syn* path with some significant exceptions. Table 2.2 reports the difference in energy barrier between *anti* and *syn*. The trend revels significant differences between *syn* and *anti* that cannot explain the magic numbers found in our experiment. Specifically, based on this trend we should not expect the presence of *anti*-6H-pentacene due to the lower barrier respect to the *syn* counterpart, whereas we might expect the *anti*-20H-pentacene due to the difficulties to a further hydrogenation. For a complete overview, see Fig. 2.8.

Table 2.2: Difference of energy barriers between the *anti* and *syn* hydrogenation ($\Delta E^{anti}{}_{bar}-\Delta E^{syn}{}_{bar}$). H*n* indicates the number of extra hydrogens chemisorbed on pentacene.

H*n*	$\Delta E^{anti}{}_{bar}-\Delta E^{syn}{}_{bar}$ (eV)
7	-0.070
11	0.039
13	0.010
15	0.019
21	-0.072

The *anti* path has the same trend in binding energies as the *syn* path. We show that *anti*-6H, *anti*-10H, *anti*-12H, *anti*-14H, *anti*-16H and *anti*-20H-pentacene have large binding energies (larger than 3.4 eV), while *anti*-11H and *anti*-17H have lower binding energy by 1 eV. Table 2.3 shows the difference of binding energies between *syn* and *anti* hydrogenation, indicating that the *anti* chemisorption of hydrogen atoms might be more favourable for some hydrogenations.

Some hydrogenation steps are not included in Table 2.3 as the energy differences are small (~0.007 - 0.09 eV). The observed pattern of magic numbers in the hydrogenation of pentacene adsorbed on graphite is fully consistent with our expectation that, because of steric reasons, hydrogenation will occur following the *syn* sequence. Specifically, we observed

Table 2.3: Difference of binding energies between the *syn* and *anti* hydrogenation of pentacene ($\Delta E^{anti}{}_{bind} - \Delta E^{syn}{}_{bind}$). H*n* indicates the number of extra hydrogens chemisorbed on pentacene.

H*n*	$\Delta E^{anti}{}_{bind} - \Delta E^{syn}{}_{bind}$ (eV)
5	0.12
10	0.24
14	0.25
16	0.17
20	0.16
22	0.30

a dominant peak at the mass of 6H-pentacene and only a minor peak corresponding to 20H-pentacene in accordance with the *syn*-sequence, but not the *anti*-sequence.

2.5. Astrophysical Implications

Massive stars have a profound influence on their nascent clouds. Specifically, far-ultraviolet photons with energies in the range 6 to 13.6 eV do not have enough energy to ionize atomic hydrogen but can photodissociate molecules and heat the gas in the surrounding molecular cloud.[146] Hydrogen is atomic in the surface layers of these so-called photodissociation regions (PDRs) while carbon is singly ionized (C^+). Going into the PDR, the dissociating and ionizing far-UV photons are attenuated by small dust grains and atomic hydrogen is converted into H_2 and, eventually, C^+ into CO. Gas temperatures in the atomic H and molecular H_2 zones of PDRs range from 200-500 K depending on star involved, while the dust is 30-75 K. Deeper in, where CO has formed, the gas cools down to 40 K. Observationally, PDRs shine brightly in the vibrational transitions of UV-pumped PAH molecules, the far-infrared fine-structure transitions of abundant atoms (C^+, O), the ro-vibrational transitions of H_2, and molecular rotational lines of *e.g.*, CO.[146]

Analysis of this data has revealed that H_2 must be very efficiently made in these surface layers.[126] This is not understood as the dust in PDRs is too warm to allow efficient H_2 formation.[33] This observed efficient H_2 formation in PDR surfaces has been ascribed to the catalytic activity of PAHs and detailed studies have appeared in the astronomical literature.[41,147–149] The present study is geared towards elucidating the interaction of atomic H with PAHs and quantitative measuring of the molecular parameters involved that are needed for these astronomical models. Our results show that addition of the first two hydrogens will be very efficient as the energy barriers involved are small and the kinetic temperature of the gas is quite high. However, adding the third hydrogen has a prohibitive energy barrier

(Fig 8) even at gas temperatures relevant for PDRs (200-500 K). To estimate the importance of quantum mechanical tunneling, we have evaluated the cross-over temperatures for the reactions involved and these are reported in the Appendix. Typically these vary from 136 to 213 K and hence, quantum mechanical tunneling is not expected to play a role in the warm gas of PDRs but it may play more of a role in cold molecular cloud. We note also that the binding energies of these extra H's are relatively low and these are readily lost in strong radiation field of a PDR.[41,148] Detailed astronomical modeling will be required to assess the balance of reactions of atomic H with PAHs and the UV photolysis in a PDR environment as well as the importance of hydrogenation of PAHs in PDRs for the formation of H_2. The experimental and theoretical results reported here will form the basis for such a modeling effort. We defer this to a follow up study that will be reported in an appropriate journal.

2.6. Discussion and Conclusion

The experimental and theoretical study conducted here has elucidated the steps that will be relevant for the hydrogenation of pentacene. We do stress that the goal of this study is to provide fundamental parameters, as energy barriers and binding energies, useful for astronomical modeling such as Andrews *et al.* addressed for coronene's family.[41] In fact, in space, superhydrogenation of PAHs is a balance between H addition and UV photolysis, energy barriers and binding energies will each play their role in setting the hydrogenation pattern of PAHs in space.

Specifically, we found that even hydrogenated species of pentacene are more preferred than the odd hydrogenated species since chemisorbing odd hydrogens on pentacene leads to the formation of reactive open-shell radicals. These extremely reactive species interact with further hydrogen atoms forming preferred species (species with magic numbers seen to dominate in mass spectra). The analysis of binding energies and energy barriers carried out in this study have confirmed the validity of the hypercoordination and coordination rule (discussed in detail in the Appendix), demonstrating that these simple concepts are applicable to small condensed and linear systems. These concepts are validated for systems formed by hexagonal aromatic rings and are applicable during the hydrogenation sequence for all benzene-like structures that still present bipartite lattices. However, we emphasize that these simple concepts are useful tools and can guide the choice of hydrogenation sites, but they cannot replace a deeper analysis of binding energies and energy barriers. Specifically, energy barriers calculation provide insights into the hydrogenation sequence, showing which species are more likely to form. We found that the energy barrier required for hydrogenating an aliphatic carbon is lower (<0.13 eV) than the energy required for hydrogenating aromatic carbons (up to 0.15 eV). Hence, the presence of magic numbers in the mass spectra are explained by the energy barriers rather than the binding energies. In fact, the absence in the mass spectra of the peaks corresponding to the masses of 12H, 14H, 18H and 20H-pentacene was confirmed by our theoretical calculations since a further hydrogenation (11H, 13H, 17H and 19H-pentacene) requires the highest energy barrier, up to 0.16 eV. Our theoretical results also suggest that both *anti* and *syn* confirmations are possible in the gas phase. The sequence found for the syn-path in our calculation matches the magic numbers found in the mass spectra for the hydrogenation of pentacene, whereas the *anti*-path might be more relevant for the hydrogenation sequence that will occur in the gas phase.

Furthermore, we noticed differences in the hydrogenation sequence that occurs in pentacene with respect to pericondensed PAHs such as coronene.[40] The hydrogenation scheme tends at first, in these aromatic molecules, to break the aromaticity of the central aromatic ring of pentacene through addition to solo sites. In contrast in coronene, where such sites are not present, this occurs for the aromatic rings located at the edges. Moreover, pentacene is more reactive at the first hydrogenation with a barrier of only 109 meV with respect to coronene.[40] As a last difference, coronene has a barrierless reaction for the addition of the last odd hydrogen. Therefore, zig-zag edges are significantly more reactive for the first hydrogen addition reaction with respect to pericondensed PAHs.

We also discovered a pathway that leads to the formation of quasi-nanotubular structures during the hydrogenation of pentacene in the gas phase. This is due to the formation of two topologically separated structures in the molecule. The two unpaired electrons located in two different systems cannot be shared any longer. Therefore, a spontaneous curling up of the structure occurs with the formation of a quasi-nanotube.

We discovered that the flexibility of the molecule provides extra structural stability with respect to more rigid molecules as coronene or graphene. Zigzag edges present on linear and flexible molecules may provide extra reactivity that may correlate the presence of H_2 with the formation of superhydrogenated species.

2.7. Appendix

In this appendix, we explain in detail the hydrogenation sequence that leads to the formation of *syn*-full-hydrogenated pentacene. We adopted the *syn* reaction sequence for the *anti*-path to enable direct comparison between two different routes. We assume that any variation in the sequence is due to the variation of the electronic structure when other positions are hydrogenated and that sequence does not change due to the orientation of the hydrogen on the molecule with respect to the molecular plane. For simplicity, we did not correct binding energies for ZPE and BSSE since these binding energies are required only for justifying the selection rules for each hydrogenation step. The energy barriers are corrected at ZPE, but not for the BSSE, since frequency analysis is necessary in order to characterize saddle points.

Hydrogenation Sequence

1st Hydrogenation

Pentacene is a symmetric molecule ($C_{22}H_{14}$, D_{2h} point group) as shown in Fig. 2.10. Initially, due to the high symmetry of the molecule, there are six possible positions where the first additional hydrogen might chemisorb as shown by C(1a-1f) in (Fig. 2.10). We can distinguish between carbon atoms that are bound to a single hydrogen atom (edge carbons) and those at inner edge sites not bound to a hydrogen atom (bridge carbons). All edge carbons have a high coordination of 2 with C(1a), C(1b) and C(1d) having hyper-coordination values of 2. C(1c) is less hyper-coordinated with a value of one. The binding energies reported in Table 2.4 shows that C(1a) and C(1b) are the most reactive and exoergic sites and are thus preferred for the first hydrogen addition, in line with the hyper-coordination rule. The calculated binding energies are in agreement with those calculated by Rasmussen using PBE.[124] We note that the C(1a) site on pentacene is significantly more reactive than the edge sites of coronene which have a binding energy of 1.16 eV.[17]

Our results are in line with the study carried out by Bonfanti *et al.*[137] since a hydrogen atom prefers to bind in a site with a high hyper-coordination number as consequence of electronic localization in a re-normalized lattice. The difference in binding energy between C(1a) and C(1b) is 0.17 eV, while the energy barriers for chemisorbing hydrogen atoms on C(1a) and C(1b) are 0.078 eV and 0.097 eV, respectively. This means that both C(1a) and C(1b) are possible sites for the first additional hydrogen atom, but C(1a) site is preferred. The hydrogenated species through this addition is referred to as 1H-pentacene in the subsequent sequence.

2nd Hydrogenation

It is well known that the chemisorption of the first additional hydrogen atom results in a favourable addition for a second hydrogen atom through a barrierless reaction resulting in a high binding energy. This has been demonstrated previously for a range of neutral and cationic PAHs.[17,128,145] 1H-pentacene is an open shell radical with singlet multiplicity. The system is characterized by a mid-gap state generated by a singly occupied molecular orbital that will react readily through a barrierless radical-radical reac-

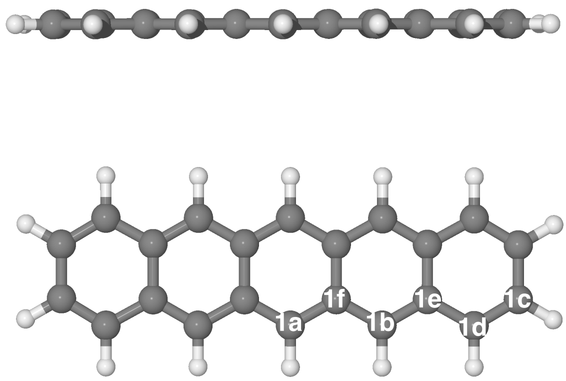

Figure 2.10: Side view and top view of the optimized molecular structure of pentacene. The alpha-numerical labels show the sequences of the possible carbon sites where an atomic hydrogen might chemisorb.

Table 2.4: Binding energies (ΔE_{bind}) for the hydrogenation of different carbon sites of pentacene. Binding energies (*) calculated by Rasmussen [124] are reported for comparison.

C site	ΔE_{bind} (eV)	Rasmussen [124]
C(1a)	2.61	2.40*
C(1b)	2.44	2.29*
C(1c)	1.81	1.79*
C(1d)	1.71	1.70*
C(1e)	0.93	0.86*
C(1f)	0.54	0.53*

tion with another radical species, such as a hydrogen atom. The mid-gap state generated is localized in the *ortho* and *para* positions with respect to the first added hydrogen atom, through Lewis resonance. This is confirmed by the trend in the calculated binding energies as shown in Table 2.5. We also considered addition to the meta positions. In this case, during the geometry optimization, the meta site hydrogen atoms were transferred from the bridge carbon to the neighbouring singly hydrogenated carbon site as shown by the red arrows in Fig. 2.11.

The calculated binding energy decreases for second addition sites far from the first hydrogenated carbon atom since the influence of the mid-gap state decreases with $1/r$. The calculations reveal that C(2a), in the *para* position, is most favourable site for the addition of a second hydro-

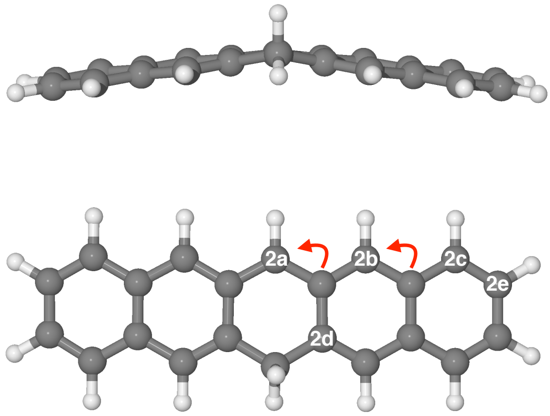

Figure 2.11: Side view and top view of the optimized molecular structure of 1H-pentacene. The alpha-numerical labels show the sequences of the possible carbon sites where a further atomic hydrogen might chemisorb.

Table 2.5: Binding energies (ΔE_{bind}) for the addition of a second extra hydrogen considering different carbon sites of 1H-pentacene.

C site	ΔE_{bind} (eV)
C(2a)	3.67
C(2b)	2.98
C(2c)	2.04
C(2d)	1.94
C(2e)	0.29

gen atom. The resulting product is 6,13-dihydropentacene (2H-pentacene) with two additional hydrogen atoms, a *para* configuration across the central hexagonal ring in a quasi-planar structure as shown in Fig. 2.12.

3rd Hydrogenation

The chemisorption of two extra hydrogen on the pentacene molecule results in a species consisting of two naphthalene units that are topologically disconnected in the same lattice. Since these two intramolecular napthalenes are equivalent and symmetric, we considered just five carbon sites for the chemisorption of the third additional hydrogen atom. C(3a) and C(3b) both present a hyper-coordination number of 2 and essentially equal binding energies (Table 2.6). Hydrogen chemisorption on either carbon site would be a valuable pathway to follow. Hence, we have selected to study the pathway initiated by hydrogen chemisorption on C(3a), but we expect that hydrogen chemisorption on C(3b) leads to comparable results. Sites (3d) and C(3c) have a hyper-coordination number of 1 and are, therefore, favourable for further addition. The calculated binding energies reported in Table 2.6, confirm the prediction of the hyper-coordination rule. The resulting structure of 3H-pentacene is a curved aromatic-aliphatic molecule, as shown in Fig. 2.13.

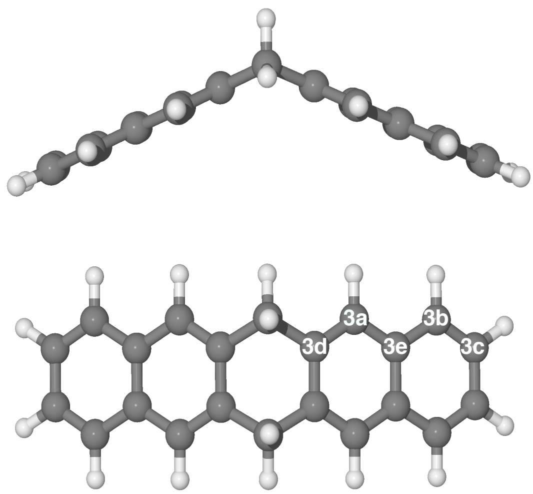

Figure 2.12: Side view and top view of the optimized molecular structure 2H-pentacene. The alpha-numerical labels show the sequences of the possible carbon sites where a further atomic hydrogen might chemisorb.

Table 2.6: Binding energies (ΔE_{bind}) for the addition of a third extra hydrogenation in different carbon sites of 2H-pentacene.

C site	ΔE_{bind} (eV)
C(3a)	1.47
C(3b)	1.43
C(3c)	1.20
C(3d)	1.03
C(3e)	0.35

4th Hydrogenation

With the formation of 3H-pentacene, a mid-gap state is again generated and localized in the associated *ortho* and *para* positions, highlighted in Fig.

2.13, as C(4a) and C(4b) sites, respectively. The difference in binding energy (E_b\{4a\} - E_b\{4b\}) is 0.04 eV, as shown in Table 2.7. We considered also the binding of a hydrogen atom to the bridge carbon adjacent to C(4a). During the geometry optimization process the additional hydrogen atom was transferred to the C(4b) site, as shown by the red arrow in Fig. 2.13. We can, therefore, state that the C(4a) and C(4b) sites are most favourable for the addition of the fourth hydrogen atom, but we selected to follow the pathway initiated by hydrogen attachment on C(4a). Also in this case, we expect that hydrogen attachment on C(4b) leads to comparable results. Less reactive sites considered are C(4d) and C(4e), characterized by planar structures associated with low binding energies since the mid-gap state decreases with distance. The geometry optimization following a addition to site C(4c) results in the formation, of a five membered-ring and three membered-ring in a curved structure shown in Fig. 2.14 and labeled in yellow in order to indicate that the chemisorption of the hydrogen in this carbon site leads to the formation a different structure. This ring arrangement has a formation energy of -1.22 eV and it is unlikely to form and will therefore not be considered for further addition.

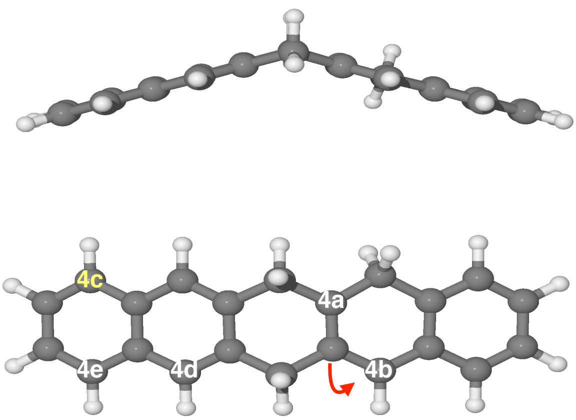

Figure 2.13: Side view and top view of the optimized molecular structure of 3H-pentacene. The alpha-numerical labels show the sequences of the possible carbon sites where a further atomic hydrogen might chemisorb.

5th Hydrogenation

In the case of 4H-pentacene the coordination rule dominates with respect to the hyper-coordination rule since the addition of the 4th hydro-

Table 2.7: Binding energies ΔE_{bind} for the addition of a fourth extra hydrogenation in different carbon sites of 3H-pentacene.

C site	ΔE_{bind} (eV)
C(4a)	3.62
C(4b)	3.58
C(4d)	0.72
C(4e)	0.24

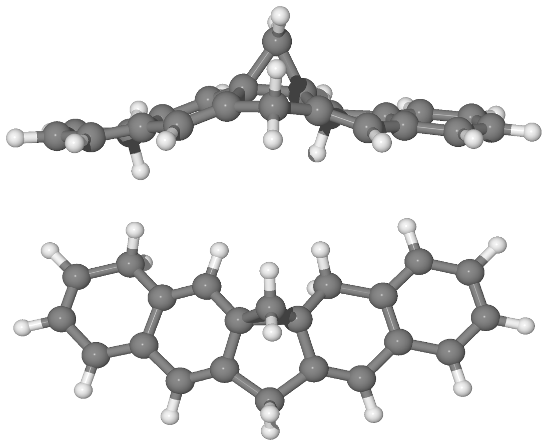

Figure 2.14: Optimized molecular structure of 4H-pentacene with a structure formed by the presence of five and three membered-rings.

gen atom results in a reduction in the coordination of the adjacent bridge carbon site, labeled 5a in Fig. 2.15, hence the fifth additional hydrogen atom prefers to bind on C(5a). This prediction is confirmed by the calculated binding energy trend shown in Table 2.8. This system presents two topologically disconnected structures, not counting the carbon atoms with two hydrogen atoms chemisorbed. We can see a naphthalene-like structure and a benzene ring-like structure, along with an aliphatic chain-like structure in the same carbon network. The hydrogen atom prefers to bind to an aliphatic rather than aromatic carbon with C(5b) being the second most favourable site. Finally, the less favourable sites belongs to the naphthalene-like structure C(5d), with a hyper-coordination number of 1. While in the benzene like structure C(5e) and C(5c) present low energy barrier respect to C(5b) and C(5a). The latter leads to the formation of the 5H-pentacene structure shown in Fig. 2.16.

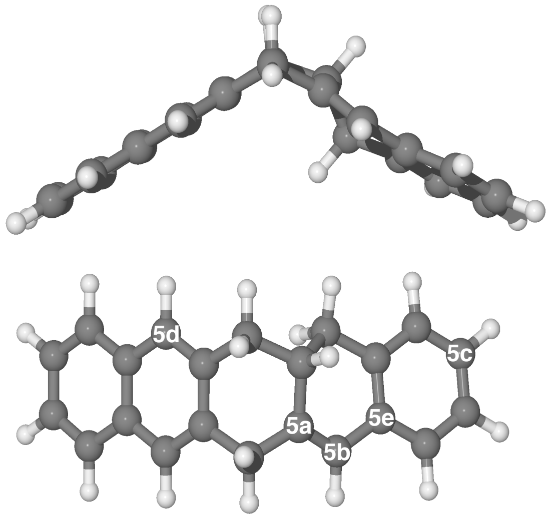

Figure 2.15: Side view and top view of the optimized structure of 4H-pentacene. The alpha-numerical labels show the sequence of the possible carbon sites where a further atomic hydrogen might chemisorb.

Table 2.8: Binding energies (ΔE_{bind}) for the fifth hydrogenation of pentacene considering different carbon sites.

C site	ΔE_{bind} (eV)
C(5a)	1.83
C(5b)	1.57
C(5c)	1.44
C(5d)	1.29
C(5e)	0.78

6th Hydrogenation

The mid-gap state generated due to the addition of the fifth atomic hydrogen leads to the chemisorption of the sixth hydrogen atom on C(6a) as shown in Fig. 2.16 with a high binding energy of 4.16 eV. While, site C(6b) shows a lower binding energy (2.82 eV). Since the system consists of two topologically disconnected structures, the trend of binding energies reported in Table 2.9 shows that the mid-gap state cannot be localized on the naphthalene-like structure. Of all sites in this region of the molecule, C(6c) has the largest binding energy as a result of having a hyper-coordination number of 2, whereas the other carbon sites have close to zero or even, in some cases such as C(6f), negative binding energies.

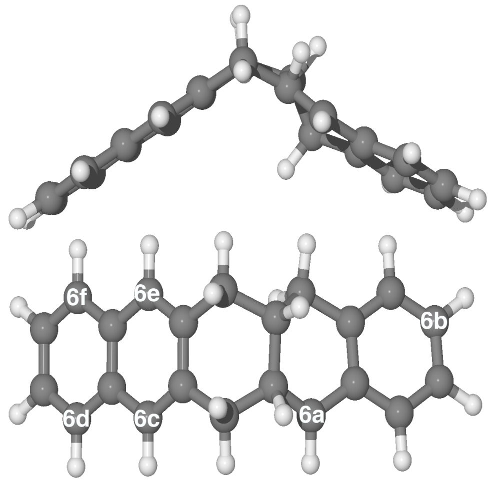

Figure 2.16: Side view and top view of the optimized structure of 5H-pentacene. The alpha-numerical labels show the sequences of the possible carbon sites where a further atomic hydrogen might chemisorb.

Table 2.9: Binding energies (ΔE_{bind}) for the sixth hydrogenation of pentacene considering different carbon sites.

C site	ΔE_{bind} (eV)
C(6a)	4.16
C(6b)	2.82
C(6c)	2.58
C(6d)	0.22
C(6e)	0.13
C(6f)	-0.14

7th Hydrogenation

We can again view the system as a structure formed by a naphthalene-like and a benzene-like ring (see Fig. 2.17). The values reported in Table 2.10 show that C(7e), C(7h), C(7f) and C(7g) are associated with the lowest binding energies and are those having a hyper-coordination number of 1. Instead, the carbons with the highest hyper-coordination number, *i.e.* 2, are, in order of decreasing binding energy, C(7a), C(7b), C(7c) and C(7d). With the formation of 7H-pentacene, the structure begins to twist on itself as shown in Fig. 2.18 where the preferred hydrogenation sites are located on the planar naphthalene unit.

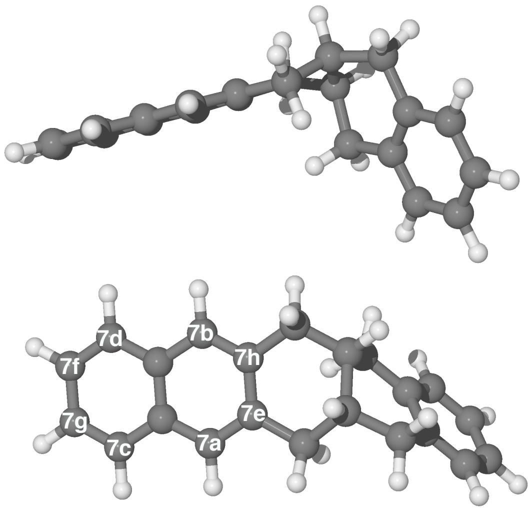

Figure 2.17: Side view and top view of the optimized structure of 6H-pentacene. The alpha-numerical labels shows the sequences of the possible carbon sites where a further atomic hydrogen might chemisorb.

Table 2.10: Binding energies (ΔE_{bind}) for the seventh hydrogenation of pentacene considering different carbon sites.

C site	ΔE_{bind} (eV)
C(7a)	1.55
C(7b)	1.54
C(7c)	1.45
C(7d)	1.45
C(7e)	1.27
C(7f)	1.22
C(7g)	1.22
C(7h)	1.06

8th Hydrogenation

Binding energies for the addition of the eighth hydrogen atom are reported in Table 2.11. The mid-gap state is localized preferentially on C(8a) or C(8b) within the naphthalene-like structure. This reactivity is also evidenced in Fig. 2.18 where the red arrows show the transfer of the added hydrogen atom to the *ortho* or *para* sites during the geometry optimization if the atom is initially placed at the adjacent bridge (meta) sites. If the eighth hydrogen is, instead, added to C(8h) and C(8i) a negative binding energy results, indicating an unfavourable endoergic chemisorption process.

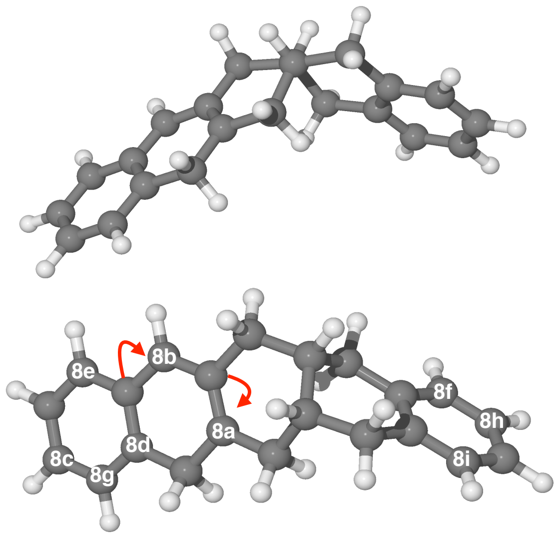

Figure 2.18: Side view and top view of the optimized structure of 7H-pentacene. The alpha-numerical labels shows the sequences of the possible carbon sites where a further atomic hydrogen might chemisorb.

Table 2.11: Binding energies (ΔE_{bind}) for the eighth hydrogenation of pentacene considering different carbon sites.

C site	ΔE_{bind} (eV)
C(8a)	3.60
C(8b)	3.58
C(8c)	2.43
C(8d)	2.31
C(8e)	2.30
C(8f)	1.14
C(8g)	0.14
C(8h)	-0.18
C(8i)	-0.19

9th Hydrogenation

In the case of addition to 8H-pentacene (see Fig. 2.19), we can view the system as a benzene ring with a carbon chain-like structure consisting of C(9b) and C(9a). These two carbons are the most reactive sites, for the chemisorption of the hydrogen, since C(9a) is the least coordinated carbon with coordination 1 (this carbon is the least coordinated carbon because it is bonded with just one sp^2 carbon, we do not consider the coordination with sp^3 carbons since they do not belong to the chain-like structure) and C(9b) is the second favourite site due to Lewis resonance. For the benzene ring formed by C(9h), C(9d), C(9g), C(9c), C(9f) and C(9e), we cannot consider the hyper-coordination rule since a benzene ring is not a bipartite lattice. The largest binding energy is associated with chemisorption on C(9c), C(9d), C(9e), while the remaining carbon sites have the lowest binding energies (i.e 9f, 9g, 9h). These values are reported in Table 2.12.

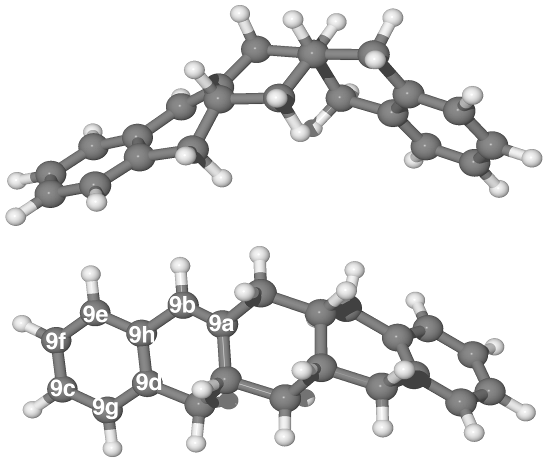

Figure 2.19: Side view and top view of the optimized molecular structure of 8H-pentacene. The alpha-numerical labels shows the sequences of the possible carbon sites where a further atomic hydrogen might chemisorb.

Table 2.12: Binding energies (ΔE_{bind}) for the ninth hydrogenation of pentacene considering different carbon sites.

C site	ΔE_{bind} (eV)
C(9a)	1.92
C(9b)	1.58
C(9c)	1.29
C(9d)	1.26
C(9e)	1.18
C(9f)	1.06
C(9g)	1.05
C(9h)	0.63

10th Hydrogenation

In the case of addition to 9H-pentacene, the mid-gap state is localized on the less coordinated C(10a), although it can also be localized on

C(10b), C(10d) and C(10c) by resonance. We noticed a further intramolecular transfer, during the geometry optimization, caused by the bent structure of the molecule (see the long arrow that connects two carbon sites on opposite ends of the molecule in Fig. 2.20). The bending of the molecule brings the two aromatic rings together, promoting a hydrogen transfer, intramolecularly, from one ring to another. The reactivity of C(10a) and C(10d) is also evidenced by the observed transfer of chemisorbed hydrogen atoms to these sites when they are attached in neighbouring bridge carbon sites as shown in Fig. 2.20. When the hydrogen atom is attached to C(10g) the chemisorption process is endoergic with a negative binding energy (Table 2.13), whereas chemisorption on C(10e) results in the formation of an intramolecular C(10g)-C(10f) bond (Fig. 2.21), with a length of 1.50 Å, during the geometry optimization. The formation of this intramolecular bond leads to the formation of an unsaturated nanotubular structure with a formation energy of -1.20 eV. Chemisorbing an atomic hydrogen on C(10a) leads to the formation of 10H-pentacene.

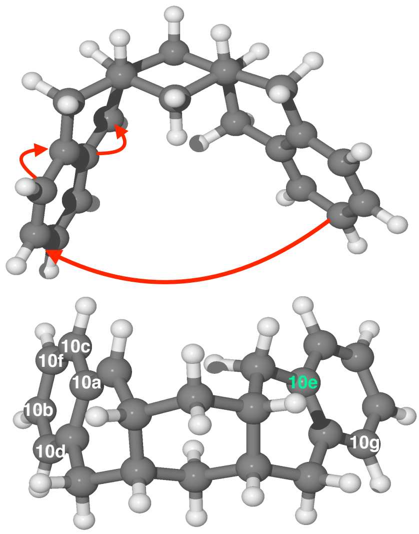

Figure 2.20: Side view and top view of the optimized structure of 9H-pentacene. The alpha-numerical labels shows the sequences of the possible carbon sites where a further atomic hydrogen might chemisorb.

11th Hydrogenation

The 10H-pentacene (see Fig. 2.22) has a structure formed by two topologically disconnected and equivalent benzene-like rings formed by C(11a)-C(11b)-C(11j)-C(11i)-C(11c)-C(11k) and C(11d)-C(11e)-C(11h)-C(11f)-C(11g)-C(11l). The two benzene rings topologically have equivalent

Table 2.13: Binding energies (ΔE_{bind}) values of the tenth hydrogenation of pentacene considering different carbon sites.

C site	ΔE_{bind} (eV)
C(10a)	3.84
C(10b)	2.79
C(10c)	2.65
C(10d)	2.45
C(10f)	0.15
C(10g)	-0.39

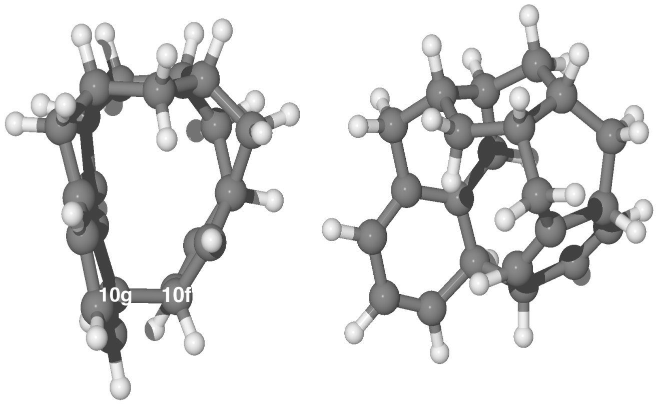

Figure 2.21: Optimized molecular structure of the quasi-nanotube 10H-pentacene formed when the 10th additional hydrogen chemisorbs on C(10e).

sites. In particular, as reported in Table 2.14, the binding energies are equal for C(11a) and C(11b), while the equivalent most reactive sites C(11e) and C(11d), in the opposite benzene-like ring, present small differences of binding energies. Instead, C(11c) and C(11i) are the second most reactive sites, or equivalently C(11f) and C(11g), since they are mirror images for symmetry. The less reactive sites are C(11k), C(11J), C(11l) and C(11h), respectively. Therefore due to the presence of carbon sites with the same binding energy, we also considered the calculated energy barriers, as reported in Table 2.15. Specifically, this shows that C(11a) has the lower energy barrier. C(11d) shows the same energy barrier as C(11a), especially in the geometrical structure of the transition state. The same applies to C(11b) and C(11c), while, C(11f) has the higher energy barrier. Therefore, we chose to proceed with the sequence from the structure obtained by chemisorbing the hydrogen on C(11a). At this stage of the sequence, it is impossible to predict further hydrogenation using the hyper-coordination rule since the two benzene rings are not bipartite lattices. The coordination and Lewis resonance rules, however, remain valid.

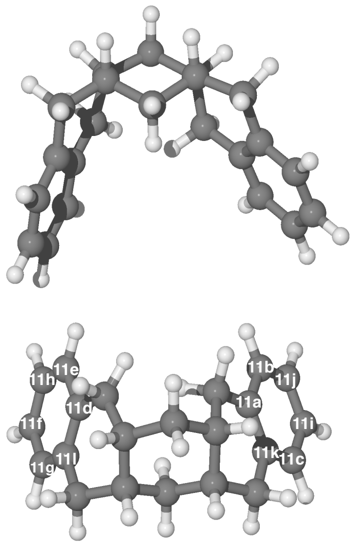

Figure 2.22: Side view and top view of the optimized structure of 10H-pentacene. The alpha-numerical labels show the sequences of the possible carbon sites where a further atomic hydrogen might chemisorb.

Table 2.14: Binding energies (ΔE_{bind}) for the eleventh hydrogenation of pentacene considering different carbon sites.

C site	ΔE_{bind} (eV)
C(11a)	1.15
C(11b)	1.15
C(11c)	1.14
C(11d)	1.12
C(11e)	1.10
C(11f)	1.08
C(11g)	1.07
C(11h)	1.05
C(11i)	1.05
C(11j)	0.99
C(11k)	0.91
C(11l)	0.99

Table 2.15: Energy barriers (ΔE_{bar}) for the eleventh hydrogenation of pentacene considering different carbon sites.

C site	ΔE_{bar} (eV)
C(11a)	0.22
C(11b)	0.23
C(11c)	0.23
C(11d)	0.22
C(11f)	0.28

12th Hydrogenation

The hydrogenation sequence continues with the attachment of the 12th additional hydrogen at the *ortho* position C(12a) as shown in Fig. 2.23. The carbon sites labeled in green indicate hydrogenation sites that lead to the formation of a quasi-nanotube, while the yellow one indicates the formation of a three-membered ring. The binding energies for the *ortho* [C(12b), C(12c)] and *para* [C(12a)] positions are shown in Table 2.16. Chemisorbing a hydrogen on the carbon located between 12b and 12a leads to the transfer of the hydrogen to C(12a) since this is the most reactive site (see short red arrow in Fig. 2.23). Hydrogen chemisorption in the carbon sites labeled in Table 2.17 leads to the formation of a biradical system that forms an intramolecular C-C bond with the creation of a nanotubular structure (see Fig. 2.24).

Table 2.16: Binding energies (ΔE_{bind}) for the 12th hydrogenation of pentacene in different carbon sites.

C site	ΔE_{bind} (eV)
C(12a)	3.49
C(12b)	3.46
C(12c)	3.44

Table 2.17: Formation energy (ΔE_f) of quasi-nanotubes (from 12d to 12h) and pentacene with a three membered-ring (12i).

C site	ΔE_f (eV)
C(12d)	2.39
C(12e)	2.38
C(12f)	2.33
C(12g)	2.01
C(12h)	1.83
C(12i)	1.62

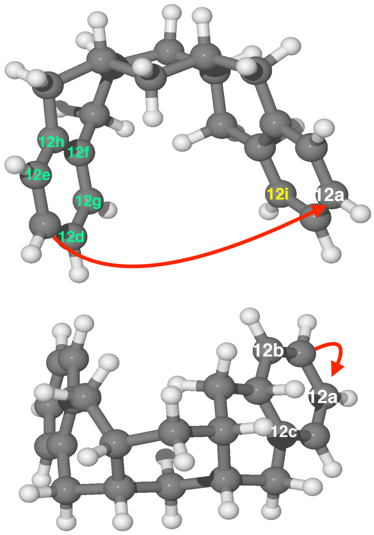

Figure 2.23: Side view and top view of the optimized molecular structure of 11H-pentacene. The alpha-numerical labels show the sequence of the possible carbon sites where a further atomic hydrogen might chemisorb.

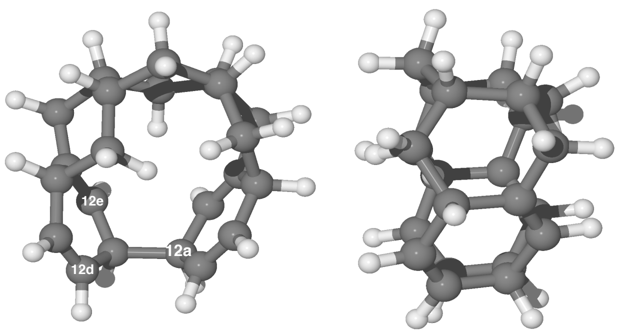

Figure 2.24: Front view and side view, respectively, of the optimized molecular structure of quasi-nanotube formed due to the chemisorption of an extra hydrogen on C(12d).

13th Hydrogenation

12H-pentacene is characterized by a bent structure with a single aromatic ring and an aliphatic diene-like ring, as shown in Fig. 2.25. Considering the calculated binding energies in Table 2.18, we observe that the hydrogen atoms prefer to bind on the aliphatic carbon sites rather than breaking the remaining aromaticity. This is demonstrated by fact that the binding energies are lower when we consider chemisorption to carbons belonging to the aromatic ring.

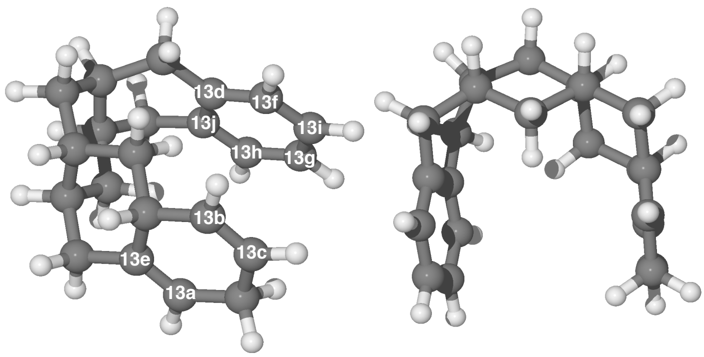

Figure 2.25: Side view and top view of the optimized molecular structure of 12H-pentacene. The alpha-numerical labels show the sequence of the possible carbon sites where a further atomic hydrogen might chemisorb.

Table 2.18: Binding energies (ΔE_{bind}) for the 13th hydrogenation of pentacene in different carbon sites.

C site	ΔE_{bind} (eV)
C(13a)	1.65
C(13b)	1.63
C(13c)	1.61
C(13d)	1.57
C(13e)	1.14
C(13f)	1.11
C(13g)	1.07
C(13h)	1.07
C(13i)	1.06
C(13j)	1.02

C(13a) is the most reactive, exhibiting a binding energy 0.02 eV larger than C(13b), and 0.04 eV larger than C(13c). The differences in energy are so small that in principle all three carbons are favourable sites for hydrogen addition. Therefore, we calculated the energy barriers for the carbon sites associated with highest binding energies, as reported in Table 2.19. These calculations confirm that C(13a) is the most reactive carbon site with the highest binding energy and lowest energy barrier. Although, C(13b), C(13c) and C(13d) show energy barriers close to the lowest value (0.13 eV), we chose to proceed with the sequence that presents the minimal energetic path. Therefore, the 13th atomic hydrogen chemisorbs on C(13a) forming 13H-pentacene.

Table 2.19: Energy barriers (ΔE_{bar}) for the 13th hydrogenation of pentacene in different carbon sites.

C site	ΔE_{bar} (eV)
C(13a)	0.13
C(13b)	0.16
C(13c)	0.17
C(13d)	0.16

14th Hydrogenation

In the case of 13H-pentacene, the only possible carbon site in which a hydrogen might bind is C(14a) since it is the least coordinated site (see Fig. 2.26). Attaching the hydrogen atom to the aromatic ring leads to negative binding energies (Table 2.20) and results in a nanotubular structure due to the formation of intramolecular biradical systems. Formation energies for such structures range from -2.50 to -2.04 eV as reported in Table 2.21. Adding a hydrogen atom to C(14b) leads to the formation of the structure shown in Fig. 2.27 which is characterized by two four membered-rings and has a formation energy of -3.07 eV. Attaching the hydrogen to the most preferred site, C(14a), thus leads to the formation of 14H-pentacene.

Table 2.20: Binding energies (ΔE_{bind}) for the 14th hydrogenation of pentacene in different carbon sites.

C site	ΔE_{bind} (eV)
C(14a)	4.15
C(14f)	0.47
C(14g)	-0.48
C(14h)	-0.56
C(14i)	-0.53

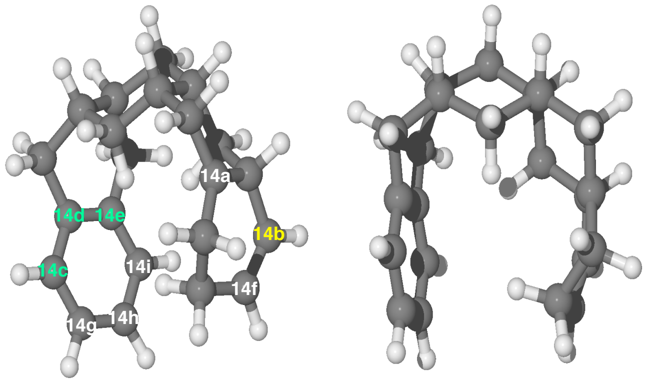

Figure 2.26: Side view and top view of the optimized molecular structure of 13H-pentacene. The alpha-numerical labels shows the sequences of the possible carbon sites where a further atomic hydrogen might chemisorb.

Table 2.21: Formation energies (ΔE_f) of quasi-nanotube (from 14c to 14e) and pentacene with two four membered-ring (14b) from 14H-pentacene.

C site	ΔE_f (eV)
C(14b)	-3.07
C(14c)	-2.50
C(14d)	-2.28
C(14e)	-2.04

15th Hydrogenation

Consistent with the previous cases, the hydrogen atom prefers to bind to the remaining two aliphatic carbons that are topologically disconnected from the aromatic ring (Fig. 2.29). This is also supported by the trend of binding energies reported in Table 2.22. It is reasonable that the system acts in this way in order to preserve the aromaticity. Attaching the hydrogen to C(15a) leads to the formation of 15H-pentacene where the remaining aliphatic rings have armchair conformation structures. Attaching an hydrogen atom on C(15b) does not change significantly the sequence since it generates a mid-gap state that is localized on C(15a). Therefore, the chemisorption of the atomic hydrogen to C(15a) or C(15b) leads to the same path of the sequence. Furthermore, the most reactive site is C(15a) with a binding energy 0.05 eV larger than C(15b). Accordingly, we proceed with the chemisorption of an extra hydrogen on C(15a) that leads to the

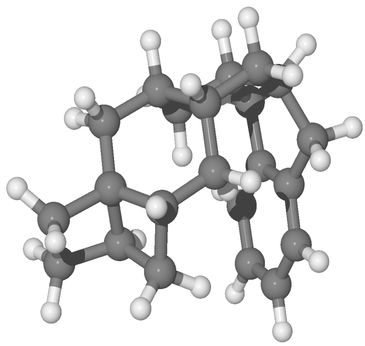

Figure 2.27: Optimized molecular structure of 14H-pentacene where the chemisorption of an extra hydrogen on C(14b) leads to the formation of two four-membered-rings.

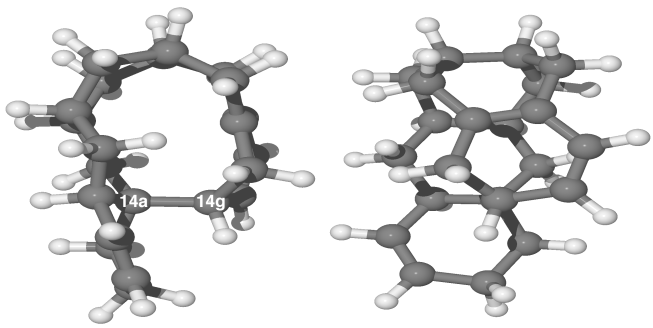

Figure 2.28: Optimized structure of the quasi-nanotube structure of 14H-pentacene formed when the 14th additional hydrogen chemisorbs on C(14c).

formation of 15H-pentacene.

16th Hydrogenation

Adding an extra hydrogen to the most favourable site of 15H-pentacene, C(16a), results in a binding energy of 4.34 eV. Binding a hydrogen atom

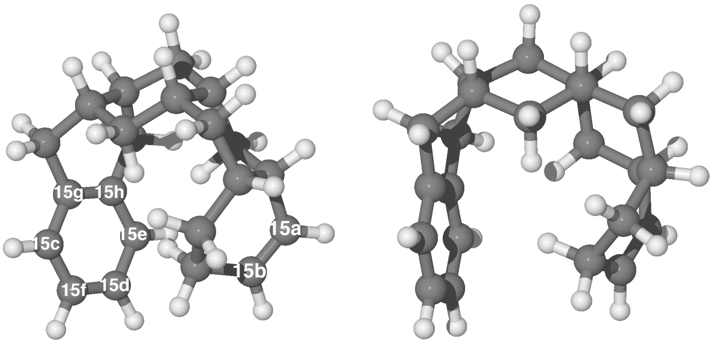

Figure 2.29: Side view and top view of the optimized molecular structure of 14H-pentacene. The alpha-numerical labels show the sequences of the possible carbon sites where a further atomic hydrogen might chemisorb.

Table 2.22: Binding energies (ΔE_{bind}) for the 15th hydrogenation of pentacene in different carbon sites.

C site	ΔE_{bind} (eV)
C(15a)	1.72
C(15b)	1.67
C(15c)	1.12
C(15d)	1.08
C(15e)	1.07
C(15f)	1.07
C(15g)	1.06
C(15h)	0.91

on one of the aromatic carbon sites, labeled in green in Fig. 2.30, leads to a singly occupied molecular orbital that results in the formation of an intramolecular C-C bond generating nanotubular structures (see Fig. 2.31) with formation energies ranging from -2.79 to -2.18 eV (see Table 2.23). Consistent with the previous case, adding hydrogen to the most reactive site C(16a) leads to the formation of 16H-pentacene.

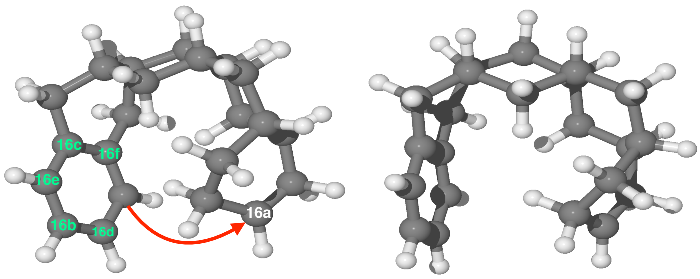

Figure 2.30: Side view and top view of the optimized molecular structure of 15H-pentacene. The alpha-numerical labels shows the sequences of the possible carbon sites where a further atomic hydrogen might chemisorb.

Table 2.23: Formation energies (ΔE_f) of quasi-nanotube.

C site	ΔE_f (eV)
C(16b)	-2.70
C(16c)	-2.54
C(16d)	-2.52
C(16e)	-2.47
C(16f)	-2.18

17th Hydrogenation

Once the pentacene molecule has reacted with 16 extra hydrogen, a single aromatic ring-like structure remains to be hydrogenated. C(17a), C(17b) and C(17c) are the most favourable sites for the 17th addition with a small difference in binding energy of 0.02 eV between C(17a) and C(17b) or C(7c). C(17b) and C(17c) are energetically equivalent. The trend in calculated binding energies is reported in Table 2.24, while, the addition sites are reported in Fig. 2.32. We continue the sequence by chemisorbing the hydrogen on C(17a) forming 17H-pentacene structure (Fig. 2.33), but we expect that hydrogen chemisorption on C(17b) or C(17c) leads to comparable results.

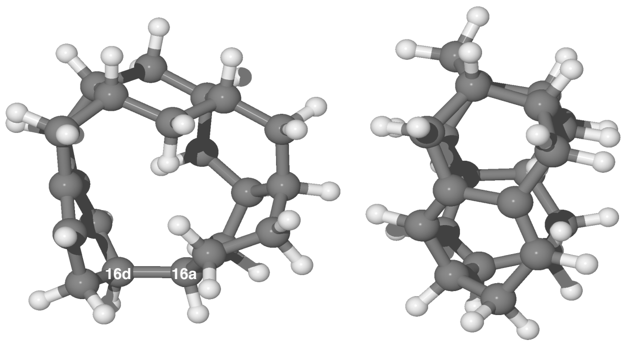

Figure 2.31: Optimized molecular structure of the quasi-nanotube structure of 16H-pentacene formed when the 16th extra hydrogen chemisorbs on C(16b).

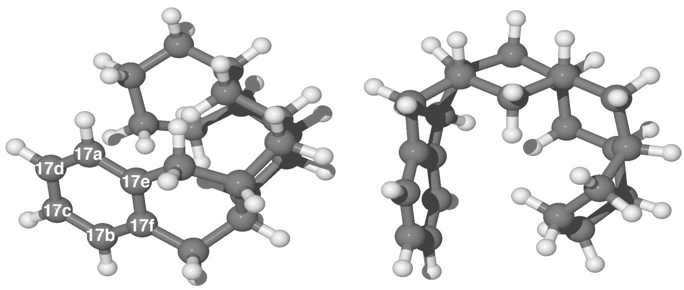

Figure 2.32: Side view and top view of the optimized molecular structure of 16H-pentacene. The alpha-numerical labels show the sequences of the possible carbon sites where a further atomic hydrogen might chemisorb.

18th Hydrogenation

The 17H-pentacene molecule has mid-gap state localized in the *ortho* and *para* positions, as shown in Fig. 2.33. Calculated binding energies

Table 2.24: Binding energies (ΔE_{bind}) for the 17th hydrogen addition to pentacene.

C site	ΔE_{bind} (eV)
C(17a)	1.10
C(17b)	1.08
C(17c)	1.08
C(17d)	1.07
C(17e)	1.05
C(17f)	0.89

are shown in Table 2.25. Similar to other cases with such a mid-gap state, the addition at the meta positions leads to the transfer of the hydrogen atom during the geometry optimization process. This confirms that C(18c) is one of the reactive sites. Attaching an hydrogen on the highlighted yellow C(18d), instead, leads to the formation of a triangle and pentagon in the same conformation structure (see Fig. 2.34) with a formation energy of -3.02 eV. The structures formed by adding a hydrogen atom to C(18a) and C(18b) have essentially equal binding energies, but we considered to chemisorb the hydrogen on C(18a). We expect that hydrogen chemisorption on either carbon site would be a valuable pathway to follow leading to comparable results.

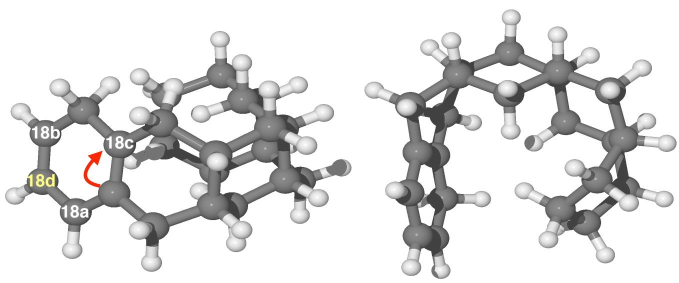

Figure 2.33: Side view and top view of the optimized molecular structure of 17H-pentacene. The alpha-numerical labels shows the sequences of the possible carbon sites where a further atomic hydrogen might chemisorb.

Table 2.25: Binding energies (ΔE_{bind}) for the 18th hydrogen on pentacene.

C site	ΔE_{bind} (eV)
C(18a)	3.48
C(18b)	3.44
C(18c)	3.36

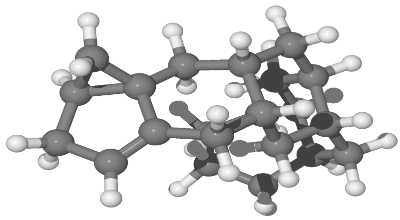

Figure 2.34: Optimized molecular structure of 18H-pentacene with a three and five membered-ring formed by the chemisorption of the hydrogen on C(18d).

19th Hydrogenation

The resulting 18H-pentacene molecule (Fig. 2.35) has four remaining aliphatic carbons which have similar values of binding energies for the addition of the 19th additional hydrogen atom, as reported in Table 2.26. Therefore, we have calculated the energy barriers as reported in Table 2.27, in order to determine the most reactive carbon site.

Based on the energy barriers, C(19d) and C(19c) have similar reactivity and so adding a hydrogen to C(19d) or C(19c) does not significantly change the sequence. If a hydrogen atom is chemisorbed on C(19c), a further hydrogen will chemisorb on C(19d) since it is then the least coordinated carbon site. Similarly, adding first to C(19d) results in the subsequent addition to C(19c). Therefore, we continue the sequence by chemisorbing the hydrogen atom on C(19c) in order to form 20H-pentacene.

Table 2.26: Binding energies (ΔE_{bind}) for the 19th hydrogen on pentacene.

C site	ΔE_{bind} (eV)
C(19a)	1.62
C(19b)	1.60
C(19c)	1.60
C(19d)	1.56

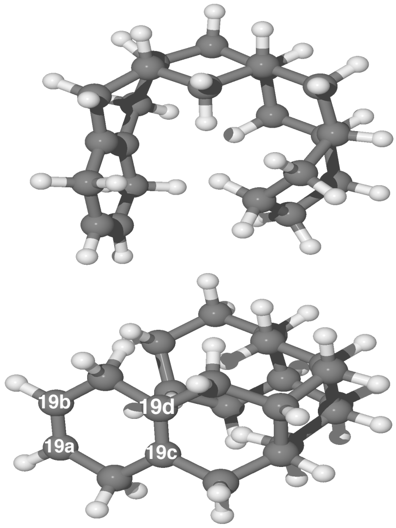

Figure 2.35: Side view and top view of the optimized molecular structure of 18H-pentacene. The alpha-numerical labels shows the sequences of the possible carbon sites where a further atomic hydrogen might chemisorb.

Table 2.27: Energy barriers (ΔE_{bar}) for the 19th hydrogen on pentacene.

C site	ΔE_{bar} (eV)
C(19a)	0.17
C(19b)	0.18
C(19c)	0.13
C(19d)	0.13

20th Hydrogenation

Fig. 2.36 shows the sites in which the 20th extra hydrogen could be added. For molecules from 19H-pentacene and beyond, the mid-gap state cannot be localized since the molecule is no longer aromatic. The most reactive carbon site is C(20a) with a binding energy of 4.27 eV. While, chemisorbing a hydrogen atom on C(20b) leads to the transfer of the already chemisorbed hydrogen on the carbon bridge between C(20c) and C(20a), to C(20c) as the arrow shows in Fig. 2.36. Adding the hydrogen to directly to C(20c) leads to a open chain structure with a exoergic formation energy of -3.39 eV, as shown in Fig. 2.37. This occurs due to the breaking of the C-C bond, formed by the CH_2 groups between C(20b) and C(20a), caused by the impossibility to localize two unpaired electrons in the same ring.

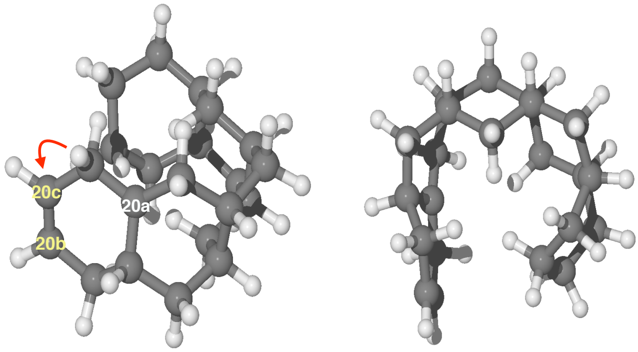

Figure 2.36: Side view and top view of the optimized structure of 19H-pentacene. The alpha-numerical labels show the sequence of the possible carbon sites where a further atomic hydrogen might chemisorb.

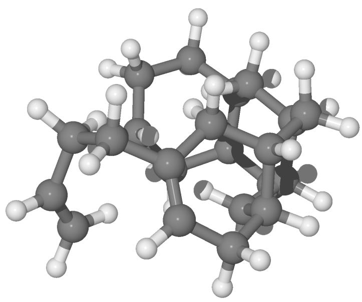

Figure 2.37: Optimized molecular structure characterized by a open aliphatic ring.

21th Hydrogenation

For the 20-H-pentacene molecule, two positions remain unhydrogenated (see Fig. 2.38). Specifically, C(21a) with a binding energy of 1.67 eV and C(21b) with a binding energy of 1.65 eV. Since the binding energies are similar, we calculated the energy barriers in order to establish the more reactive position. Specifically, adding a hydrogen on C(21a) requires overcoming an energy barrier of 0.09 eV, whereas for C(21b) the barrier is

0.16 eV indicating that the most reactive site is C(21a).

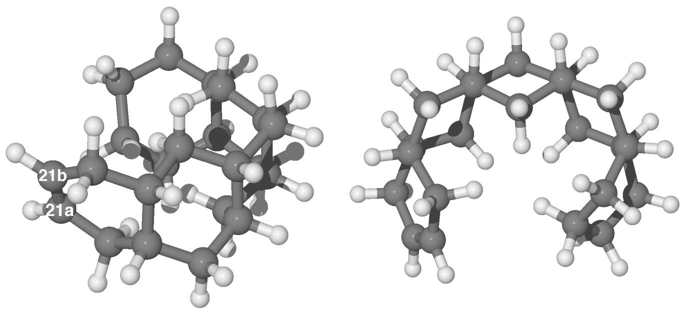

Figure 2.38: Side view and top view of the optimized molecular structure of 20H-pentacene. The alpha-numerical labels show the sequences of the possible carbon sites where a further atomic hydrogen might chemisorb.

22th Hydrogenation

After the chemisorption of the 21st hydrogen the reaming carbon available is C(21b), shown in Fig. 2.38. A hydrogen adsorbed in this final position has a binding energy of 4.20 eV forming the full hydrogenated pentacene, 22H-pentacene ($C_{22}H_{36}$).

Crossover Temperatures

In Table 3.5 are reported the values of crossover temperature (temperature below which quantum tunneling effects are important) calculated using the following expression: Tc = $(\hbar*\mathrm{freq})/k_b$. $\hbar$ is the reduced Planck's constant ($\hbar$=h/2π), freq is the module of the imaginary frequency of the transition state and k_b is the Boltzmann's constant.

Table 2.28: Values of crossover temperatures (Tc), classical TST rates (*Kc*) and the Gibbs free energies difference between the TS and the reactant at the crossover temperature ($\Delta\ G^{Tc}$) for each odd hydrogenation (H*n*) of pentacene.

H*n*	Tc (K)	*Kc* (s^{-1})	$\Delta\ G^{Tc}$ (eV)
1	136.59	16712120.68	0.14
3	199.26	136556.81	0.29
5	184.94	193213.29	0.27
7	191.13	344328.39	0.27
9	136.16	881983.68	0.17
11	213.12	10245.73	0.36
13	166.33	887483.50	0.22
15	145.71	3734276.02	0.17
17	210.82	17974.56	0.35
19	180.88	525659.29	0.25
21	167.41	941511.59	0.22

While the classical TST rate (*Kc*) has been calculated as following: *Kc* = (k_b*Tc/h)exp(-Δ G^{Tc}/R*Tc). Δ G^{Tc} is the Gibbs free energies difference between the TS and the reactant at the crossover temperature and R is the gas constant.